



OPEN

Pressure effect on stabilities of self-Interstitials in HCP-Zirconium

Qing Peng¹, Wei Ji¹, Jie Lian¹, Xiao-Jia Chen², Hanchen Huang³, Fei Gao⁴ & Suvranu De¹

¹Department of Mechanical, Aerospace and Nuclear Engineering, Rensselaer Polytechnic Institute, Troy, NY 12180, U.S.A., ²Key Laboratory of Materials Physics, Institute of Solid State Physics, Chinese Academy of Sciences, Hefei 230031, China, ³Department of Mechanical and Industrial Engineering, Northeastern University, Boston, MA 02115, U.S.A., ⁴Fundamental and Computational Sciences Directorate, Pacific Northwest National Laboratory, Richland, Washington 99352, U.S.A.

The self-interstitial atoms (SIAs) mediate the evolution of micro-structures which is crucial in understanding the instabilities of hexagonal close packed (HCP) structures. Taking zirconium as a prototype, we investigate the pressure effect on the stabilities of SIAs using first-principles calculations based on density-functional theory. We found that the pressure greatly affects the stability of the SIAs. The SIAs in basal planes are more stable under pressure. The SIA configuration of the lowest formation energy changes from basal octahedral (BO) to octahedral (O) at a pressure of 21 GPa. The lowest formation enthalpy configuration switches from BO to S (split-dumbbell) at the pressure of 30 GPa. The formation volumes of SIAs decrease monotonically in response to an increase in pressure. Our results reveal that it is important to take pressure effects into account when predicting the micro-structural evolution of HCP structures.

Radiation profoundly affects the life on our planet. For protection, it is important to understand the radiation damage as well as the radiation resistance of materials. The self-interstitial atoms (SIAs) of a crystal play a significant role in the evolution of micro-structures at the nanoscale, which ultimately determines the instabilities of the materials. With the creation of a SIA, the local stresses and strains around the SIA are several orders of magnitude larger than the global stresses and strains. In addition, thermal gradient induced stresses, namely thermal stresses, are very common in micro-structures, especially around a collision cascade. Thus the pressure is an important factor in determining the stability of SIAs. For example, it was found that the hydrostatic pressure greatly influences the SIAs' formation, migration¹, and aggregation^{2,3} in silicon. However, to the authors' best knowledge, no quantitative study of the pressure effect on the stabilities of self-interstitials in hexagonal close packed (HCP) structures has been reported.

We take zirconium as the prototype HCP structures due to its importance in nuclear materials^{4–6}. When one extra atom sits inside an HCP structure, there are eight symmetrical positions in which it can rest. For a thorough study of SIA behaviors, we have studied all eight SIAs. Here we use the conventional notations for these eight configurations⁷, as octahedral (O), split $\langle 0001 \rangle$ dumbbell (S), crowdion (C), tetrahedral (T), basal octahedral (BO), basal split (BS), basal crowdion (BC), and basal tetrahedral (BT), as shown in Fig. 1. More specifically, site O is at the center of an octahedron formed by six neighbor atoms. Site S is a split dumbbell along $\langle 0001 \rangle$. Site C is the middle point between two nearest-neighbor atoms out of the basal plane. Site T is the center of a tetrahedron formed by four neighboring atoms, of which three are on the basal plane forming an equilateral triangle and the fourth is on top of the center of the triangle. The first four configurations are “off-plane” configurations as their positions are out of the basal plane. The remaining four are “in-plane” configurations, which are the projections of off-plane counterparts onto the basal plane. The stabilities of these eight SIAs were reported in our previous work, in which we concluded that the BO is the most stable configuration⁸, as confirmed by other first-principles calculations^{9,10}. A further study on the axial ratio (c/a) dependence of the stability of SIAs in HCP structures shows that the axial ratio dominates the relative stability of SIAs over volumetric strains¹¹. Below the ideal value of $c/a = 1.633$, the basal octahedral configuration is the most stable. Above the ideal value, the off-plane SIAs are more stable than in-plane ones.

At ambient conditions, pure zirconium crystallizes in HCP structure as α phase. Experiments^{12,13} found that there is a phase transition from HCP structure to another hexagonal structure (space group $P6/mmm$, #191), named ω phase, at pressure of 2–7 GPa and it will further transform to the body-centered-cubic structure as β phase at the pressure of 30–35 GPa. The phase transitions of $\alpha \rightarrow \omega$ and $\omega \rightarrow \beta$ at zero temperature have been calculated to be -3.7 GPa and 32.4 GPa, respectively⁶.

SUBJECT AREAS:

METALS AND ALLOYS

MECHANICAL ENGINEERING

STRUCTURE OF SOLIDS AND
LIQUIDS

MECHANICAL PROPERTIES

Received

2 April 2014

Accepted

18 June 2014

Published

18 July 2014

Correspondence and
requests for materials
should be addressed to
Q.P. (qpeng.org@
gmail.com)

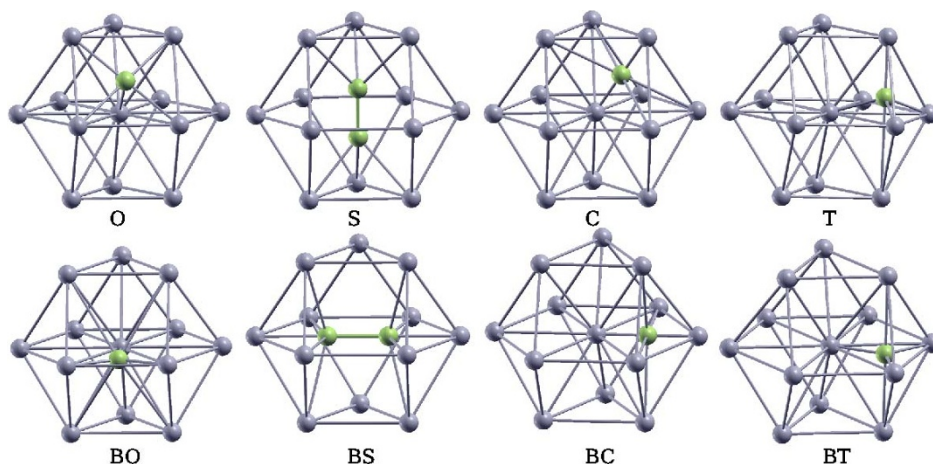


Figure 1 | Conventional eight configurations (namely O, S, C, T, BO, BS, BC, BT) of SIA (green ball) in HCP structures.

The thermodynamically relevant quantity which determines the stability under pressure is the formation enthalpy. The calculation of formation enthalpy is non-trivial, since it needs the knowledge of the formation volume and the formation energy *a priori*. Density functional theory (DFT) is well established and it can provide unique information about the structure of nanoscale defects. Involving no experimental input parameters, DFT models appear to be as quantitatively accurate and informative as the most advanced experimental techniques developed for the observation of radiation damage phenomena^{14,15}. Here we will employ DFT calculations to unveil the pressure effect on the stabilities of these eight SIA configurations as part of a series of DFT studies toward the understanding of radiation damage of zirconium. To that end, we developed a general method to calculate the formation enthalpy from *ab initio* DFT calculations through the equations of state. This method could bridge the atomic scale DFT calculations to the continuum description of the materials in terms of thermo-dynamical properties.

In the present work, we studied the pressure effect on the stabilities of SIAs by examining the eight conventional SIA configurations using *ab initio* DFT calculations. We found that the pressure greatly affects the stability of the SIAs. We also obtained the equations of state, formation volume, and formation enthalpy under pressure. This could provide insights into the SIAs' diffusion paths where the most stable configurations are considered. Our study could also be useful in engineering designs of cladding materials and structural materials that are used in the high pressure environments.

Methods

Formula for formation energy, volume, and enthalpy. To study the pressure effect on the stabilities of SIAs in HCP structures, we introduce a general method to calculate the formation volume and formation enthalpy of defects through the equations of state (EOS) using *ab initio* DFT calculations. This general method is for macroscopic constitutive descriptions from lower level quantum mechanical calculations. This EOS method was previously used in face-centered cubic (FCC) structures, differing in the forms of EOS^{16–18}. Here we extended the method to HCP structures with the justification of the applicable range.

For plane-wave based *ab initio* DFT codes, such as VASP^{19,20}, it is convenient to use constant volume boundary conditions, which ensure the same plane wave basis during a single calculation for reliable results. However, it is more reasonable to have constant pressure in experiments. This mismatch of boundary conditions makes it hard to validate the computational values with experiments. This barrier can be overcome by using the EOS, which makes it convenient to switch between the boundary conditions of constant volume and constant pressure for the computation of related quantities, including SIA formation energy, formation volume, and formation enthalpy, as discussed in the following sections.

Many analytic and semi-empirical relations have been proposed to describe the EOS for various classes of solids^{21–23}. It is generally believed that for strains less than 30%, most EOS are similar in accuracy^{24,25}. Here we use the Murnaghan EOS²¹. The pressure-volume relationship is expressed by the Murnaghan EOS as²¹

$$P(V) = \frac{B}{B'} \left(\left(\frac{V_0}{V} \right)^{B'} - 1 \right), \quad (1)$$

where V_0 is the volume at equilibrium at zero temperature and zero pressure, B is the bulk modulus, and B' is the pressure derivative of bulk modulus. Equivalently, the volume as a function of pressure is

$$V(P) = V_0 \left(1 + \frac{B'}{B} P \right)^{-1/B'}. \quad (2)$$

If DFT computations are used to calculate the total energy of the system (E) as a function of the volume (V), then the parameters in the EOS (equations Eq. 1 and 2) can be obtained by fitting with the following equation²¹

$$E(V) = E_0 + \frac{VB}{B'} \left(1 + \frac{(V_0/V)^{B'}}{B'-1} \right) - \frac{BV_0}{B'-1}, \quad (3)$$

where E_0 is a constant, marking the total energy of the system at the reference state of $P = 0$ or equivalently, $V = V_0$.

The total energy of the system at any state of volume can be obtained, by the least-square fitting process²⁶ of $E(V)$. With the values of V_0 , B , and B' from the fitting, theoretical values of the thermodynamic state quantities are known. Considering two systems, with and without SIA, we have two sets of EOS and the total energies for the two systems at all states. Thus, the formation energy, formation volume, and formation enthalpy of SIAs can be predicted. Corresponding to the boundary condition of constant pressure, the formation energy at pressure P is defined as^{1,17,18,27}

$$E^f(P) = E(N+1; P) - \frac{N+1}{N} E(N; P), \quad (4)$$

where $E(N+1; P)$ and $E(N; P)$ are the total energies of the SIA system and the ideal system (without defects), respectively, which are calculated from Eq. 2. The SIA formation volume $\Omega^f(P)$ is defined as

$$\Omega^f(P) + V(N+1; P) - \frac{N+1}{N} V(N; P), \quad (5)$$

where $V(N+1; P)$ and $V(N; P)$ are the volumes of the SIA system and the ideal system (without defects), respectively, at constant pressure P . $V(N+1; P)$ and $V(N; P)$ are calculated from Eq. 1. With the formation energy $E^f(P)$ and formation volume $\Omega^f(P)$, the formation enthalpy of SIAs can be calculated as:

$$H^f(P) = E^f(P) + P\Omega^f(P), \quad (6)$$

where $P\Omega^f(P)$ is the external work to the formation volume due to the pressure P . At zero pressure, $H^f(0) = E^f(0)$.

This method is general for solid materials due to the universal EOS applied. In this work, the volume is changed by applied volumetric strains, which are equal in all directions. The applicable range of the strains is within the $\pm 30\%$ volumetric strains^{24,25}, as shown later in this study. This EOS method is expected to be applicable for systems with other kinds of defects, including vacancy, vacancy clusters, SIA clusters, and dislocations. The advantages of this general method include the following points. First, it provides a reliable way to predict the formation energy, formation volume, and formation enthalpy of defects at a lower computational cost. Second, conversions between pressures and volumes are simple, due to the analytical formula (Eq. 1 and Eq. 2). Third, through the equations of state, it provides a new approach to study these quantities. Finally, it provides a direct comparison between



experiments and numerical simulations. Therefore, this method could be a useful tool to study the micro-structures.

Density functional theory calculations. The simulation box contains $5 \times 3 \times 3$ unit cells. Each unit cell has four Zr atoms with dimensions of $a, \sqrt{3}a, c$ and the four atoms are positioned at $(0, 0, 0)$, $(1/2, 1/2, 0)$, $(0, 1/3, 1/2)$, and $(1/2, 5/6, 1/2)$ in the reduced coordinates, where a and c are lattice constants of HCP-Zr. For the ideal structure without any defects, the simulation box is $16.19 \times 16.83 \times 15.55 \text{ \AA}^3$ with 180 atoms. Such a selection of the simulation box is to ensure that the minimum distance between the defects and their images due to the periodic boundary conditions are greater than 15.55 \AA , which makes the interactions between defects as well as the elastic dipole interactions¹⁰ negligible.

The first-principles calculations were carried out using the Vienna Ab-initio Simulation Package (VASP)^{19,20} which is based on the Kohn-Sham Density Functional Theory (KS-DFT)²⁸ with the generalized gradient approximations as parameterized by Perdew, Burke, and Ernzerhof (PBE) for exchange-correlation functions²⁹. The pseudo-potential in this study has twelve electrons ($4s^2 4p^5 5s^2 4d^2$) explicitly included as valence electrons. The core electrons are replaced by the projector augmented wave (PAW) approach³⁰.

The cutoff energy for the kinetic energy of wave-functions was carefully selected to be 400 eV after convergence tests. A gamma-centered k -mesh is required to sample the irreducible Brillouin Zone in HCP structures to preserve the HCP symmetry. Thus we used $3 \times 3 \times 3$ Γ -centered k -mesh in this study after convergence tests. The integration over eigenvalues is performed by the smearing technique using the Methfessel-Paxton function of order 1 and a smearing width of 0.05 eV³¹, which results in a convergence of total energy of 2.0 meV/cell for the largest system in this study.

With the initial atomic positions schematically shown in Fig. 1, the SIA structures are optimized using the conjugate gradient method. The criterion to stop the relaxation of the electronic degrees of freedom is that the convergence of total energy is 10^{-5} eV. The optimized atomic geometry was achieved through minimizing Hellmann-Feynman forces acting on each atom until the maximum forces on the atoms were smaller than 0.03 eV/Å. The pressures of the systems after relaxation are small, less than 0.1 GPa. All the parameters selected in this study will ensure the convergence of formation energies within 0.05 eV/cell.

Results

Lattice constants and elastic properties. The lattice constants were obtained by relaxing the primitive unit cell with a cutoff energy of 1300 eV for wave functions and a cutoff energy of 2000 eV for augmentation charges for high accuracy. The elastic tensor was determined by performing six finite distortions ($\delta\epsilon = 0.015$) of the HCP lattice and deriving the elastic constants from the strain-stress relationship, where stresses were calculated *ab initio* by properly applied strains after a convergence test of $\delta\epsilon$ ³². All internal relaxations were performed. The bulk modulus B was calculated using³³

$$B = \frac{C_{33}(C_{11} + C_{12}) - 2C_{13}^2}{C_{11} + C_{12} + 2C_{33} - 4C_{13}}, \quad (7)$$

with $C_{12} = C_{13} = C_{11} - 2C_{66}$.

The results of lattice constant a , c/a ratio, bulk modulus B , elastic constants in HCP C_{11} , C_{33} , C_{44} , C_{66} obtained from *ab initio* calculations are summarized and compared with previous studies and experiments in Table I. They are in good agreement with both experiments and previous *ab initio* calculations.

Equations of state. Nine systems were studied including eight SIAs and the ideal system (without SIA). For each system, we calculated

Table 1 | Lattice constant (a), the c/a ratio, the bulk modulus, and elastic constants (C_{11} , C_{33} , C_{44} , C_{66}) of bulk HCP Zirconium from *ab initio* DFT calculations, compared with experiment⁴⁷ and previous calculations^{39,48}

	a (Å)	c/a	B (GPa)	C_{11} (GPa)	C_{33} (GPa)	C_{44} (GPa)	C_{66} (GPa)
Present	3.238	1.600	93.6	143.5	168.5	25.5	38.8
Experiment[47]	3.23	1.593	97	144.0	166.0	33.0	35.0
Calculation[39]	3.23	1.600	94	146	156	28	42
Calculation[48]	3.24	1.598	93.4	141.1	166.9	25.8	36.8

the total energies corresponding to seven volumes. The results of $E(V)$ as a function of V are plotted in Fig. 2.

The total energies as a function of volume were fitted to Eq. 3, and we obtained the fitting parameters V_0 , B , and B' . The fitting parameters of the eight SIAs and the ideal system are summarized in Table II, as well as the errors introduced by the fittings. Our EOS parameters agree with experiments^{34,35}, where B is measured as 92–102 GPa and B' is 3.1–4.0.

Using these fitting parameters V_0 , B , and B' , the equations of state of Eq. 1 can be obtained. The pressure as a function of volumetric strain (EOS) for the ideal system using a 180-atom unit cell and eight SIAs (O, S, C, T, BO, BS, BC, BT) using scaled 181-atom unit cells were plotted in Fig. 3, where pressures of SIAs have 10.0 GPa increment each to avoid overlapping for better view. We observed that the EOS of ideal and SIA systems are very similar in a large range of the volumetric strain. We only show the P - ϵ within the volumetric strain range of -0.3 to 0.3 .

We used the pressure range of -10 GPa to 40 GPa for the study of the SIA formation energy under constant pressure $E^f(P)$, formation volume, and formation enthalpy in the following subsections. The pressure of 40 GPa corresponds to the volumetric strain of -0.227 which is 7.56% compressive strain in each direction. The pressure of -10 GPa corresponds to the volumetric strain of 0.136, which is 4.53% tensile strain in each direction.

Although there are experimentally reported phase transitions under high pressures^{12,13}, the pressure-induced phase transition was not observed in our calculations. The possible reasons are two-fold. First, the simulation boxes are small, which exclude the long wavelength phonon modes that corresponds to the soft-mode for the phase transitions. Second, the zero temperature in our model precludes the dynamical instabilities, resulting in meta-stable configurations under high pressures. Even though, our calculations are still useful in studying the mechanical instabilities of defects under various pressures since it provide an upper boundary of these instabilities. The pressure-induced phase transition can be theoretically obtained from comparison of the enthalpy of different possible atomic structures^{6,36,37}. However, it is outside the aim of present work.

It is worth pointing out that the large pressures (from -10 to 40 GPa) in this theoretical study are much larger than that in real applications, for example, 0.016 GPa in pressurized water reactors (PWR). In practice, zirconium alloys cannot sustain such high pres-

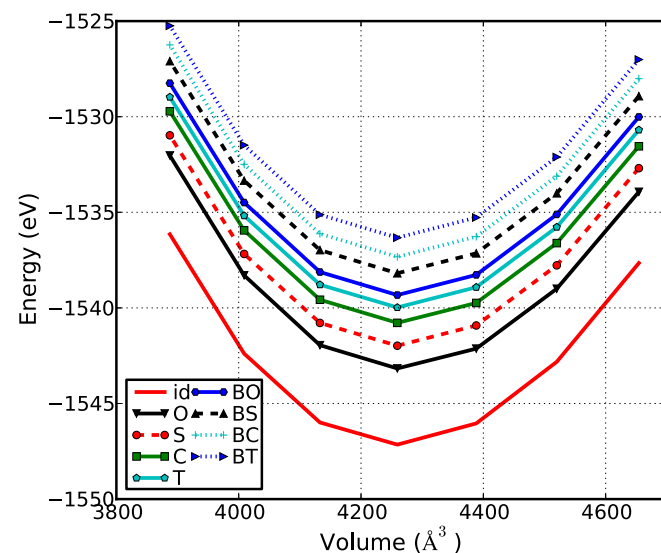


Figure 2 | The total energy as a function of volume for ideal system (red line) in a 180-atom unit cell and eight SIAs (O, S, C, T, BO, BS, BC, BT) in scaled 181-atom unit cells. The plots for SIAs systems have 1.0 eV increment each for better view.



Table II | Equilibrium volume V_0 , bulk modulus B , its pressure derivative B' , and formation energy under constant zero pressure $E^f(P=0)$ of bulk HCP Zirconium and eight SIA configurations (O, S, C, T, BO, BS, BC, BT) from EOS fitting of *ab initio* DFT calculations. The errors introduced by the least square fittings are shown in the parenthesis next to each parameter. For comparison, we listed the formation energies under constant zero pressure $E^f(\varepsilon=0)$ which were reported previously^{8,49}

	V_0 (Å ³)	B (GPa)	B'	$E_{\varepsilon=0}^f$ [8] (eV)	$E^f(P=0)$ (eV)	$E_{\varepsilon=0}^f$ [49] (eV)
ideal	4235.51 (0.12)	94.64 (0.040)	3.505 (0.026)	0	0	0
O	4262.91 (0.13)	93.83 (0.042)	3.492 (0.027)	2.98	2.98	2.88
S	4261.63 (0.14)	93.52 (0.043)	3.429 (0.028)	3.17	3.18	-
C	4262.58 (0.13)	93.50 (0.042)	3.442 (0.027)	3.37	3.37	-
T	4261.63 (0.14)	93.52 (0.043)	3.429 (0.028)	3.17	3.18	-
BO	4261.98 (0.20)	94.01 (0.065)	3.426 (0.042)	2.82	2.82	2.90
BS	4262.55 (0.11)	93.77 (0.036)	3.443 (0.024)	2.96	2.96	-
BC	4261.98 (0.20)	94.01 (0.065)	3.426 (0.042)	2.82	2.82	2.91
BT	4261.98 (0.20)	94.01 (0.065)	3.426 (0.042)	2.82	2.82	-

pressures as 40 GPa. Because there are defects including dislocations, grain boundaries, and voids during manufacture in addition to the thermal point defects. The stresses are highly and locally concentrated during mechanical loading, thermal straining, and irradiation around these defects. As a result, the pressures around the micro structures of defects are very high. For example, a shock compression of 7.56% of a unit cell (22.7% volume shrinkage) during collision cascade could cause a local pressure as high as 40 GPa. However, it is difficult to experimentally measure these localized high pressures due to following reasons. First, the pressures on those hot spots are quickly reduced with respect to the increment of distance between the defect and the measuring point, as well as the surface area of the measurement due to averaging. Second, the pressures on those hot spots are instantaneous and promptly dissipated, in order of 10^{-12} s (picoseconds). Therefore, our theoretical studies at the nanoscale and high pressures are valuable since it provides the sights of mechanical behaviors which are difficult to capture in experimental approach since they are instantaneous and highly localized. In addition, it also provides insights into the stabilities as well as the

phase transition path which consists of the configurations of lowest formation enthalpy.

The direct DFT calculations of the ideal system's pressure with respect to the volume are also plotted as red dots in the bottom panel of Fig. 3. It verifies that the EOS from Eq. 1 fits the DFT results well and thus it is reliable for use in calculation of SIA formation energy, formation volume, and formation enthalpy, as discussed in the following subsections.

Formation energy. The formation energy is the energy cost of generating a defect configuration, which is used to quantify the stability of a SIA configuration as compared with the ideal system without any defects. The difference in formation energy between two SIAs is a measure of the relative stability between them. The formation energies of SIAs at constant pressure $E^f(P)$ as a function of pressure P are plotted in Fig. 4 with the parameters in Table II. Under positive pressures, where the system is in the compression mode, the distances between atoms are reduced. As a result, the strength of the bonds is enhanced. It requires more work to insert the SIA atoms to the system, thus the formation energy increases. Under negative pressures, where the system is in the expansion mode, the distance between atoms increases. As a consequence, the bonds are weakened. The insertion of the SIA increases the strength of bonds, and thus increase the formation energy.

The formation energies at zero pressure $E^f(P=0)$ are summarized in Table II. The formation energy at constant pressure $E^f(P=0)$ is identical to the $E^f(\varepsilon=0)$, formation energy at constant volume,

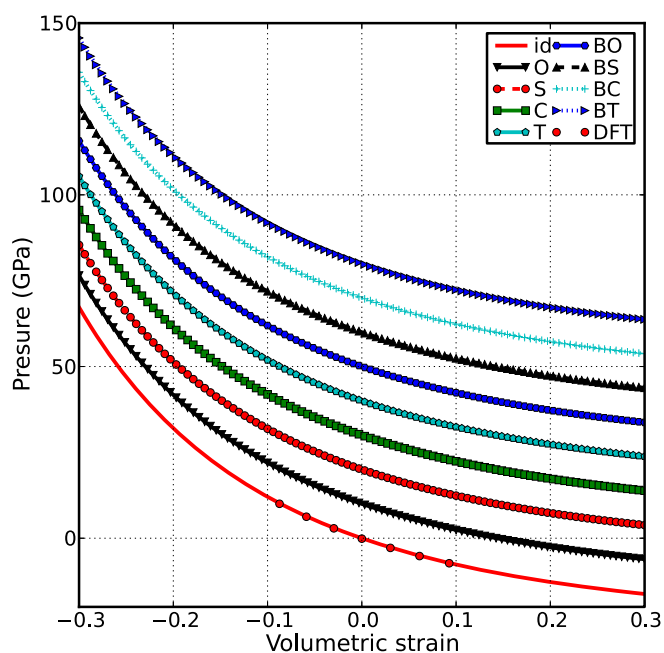


Figure 3 | The pressure as a function of volumetric strain (EOS) for ideal system (red line) in a 180-atom unit cell and eight SIAs (O, S, C, T, BO, BS, BC, BT) in scaled 181-atom unit cells. The pressures of SIAs have 10.0 GPa increment each to avoid overlapping for better view.

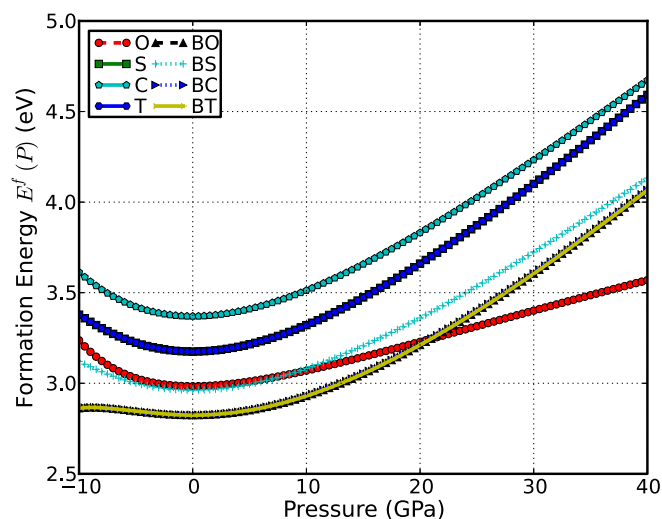


Figure 4 | Formation energy of eight SIAs (O, S, C, T, BO, BS, BC, BT) at constant pressure $E^f(P)$ as function of pressure P .



calculated from the rescaled constant volume method^{18,38,39}. This is also a direct validation of the rescaled constant volume method used in our previous works^{8,11}. The crossovers of $E^f(P)$ curves for different SIAs only occur at pressure $P > 8$ GPa. The lowest-conformation-energy configuration changes from BO to O at pressures $P = 21$ GPa with an increase of pressure. This is consistent with our observations of the behaviors of $E^f(\epsilon)$.

It is worth mentioning that the formation energy of each SIA configuration strongly depends on the system size⁸. The general trend is that the formation energy decreases as the system size increases. It is well known that the interactions between the SIAs and their periodic images, which are caused by the periodic boundary conditions, are artificial. These artificial interactions are the main cause of inaccuracy of formation energy appeared as a system size effect in modeling. These interactions decay quickly with respect to the distances between the nearest defects. As reported in our previous study⁸, the SIA formation energy converges when the number of atoms of the system $N \geq 180$, where the shortest distance between defects is no smaller than 15.55 Å.

Formation volume. The SIA formation volume measures the volume change of the SIA system with respect to the ideal system at the same condition of N and P . Under the constant pressure P , since the electrons are delocalized in metals, the system volume determines the overall binding energy in the system. As a result, the formation volume contributes to the bonding and thus the formation energy.

Formation volumes of SIAs at constant pressure $\Omega^f(P)$ as a function of pressure P are shown in Fig. 5. The unit of $\Omega^f(P)$ is $\Omega_0 = V(N; P = 0)/N$, which is the unit atom volume at zero pressure of the ideal system for convenience. In this study, we have $\Omega_0 = 23.52 \text{ \AA}^3$. The formation volume at zero pressure $\Omega^f(0)$ is summarized in Table III. Our values are comparable to the first principles calculations in 96-atom super-cells^{10,40} and consistent with experiments. Comparing with empirical many-body potentials, our results are smaller than those reported by Ackland *et al.*⁴¹, but larger than those of Pasianot and Monti⁴². Note that there are big differences in formation volume between these DFT results, even a change of sign, which could be due to the small system size (37 or 97 atoms) used in previous DFT models.

The general trend is that the $\Omega^f(P)$ decreases with pressure. This could be understood since the total volume decreases with pressure. At the higher pressure, the system is “denser” and the SIAs are more constrained to vibrate and relax.

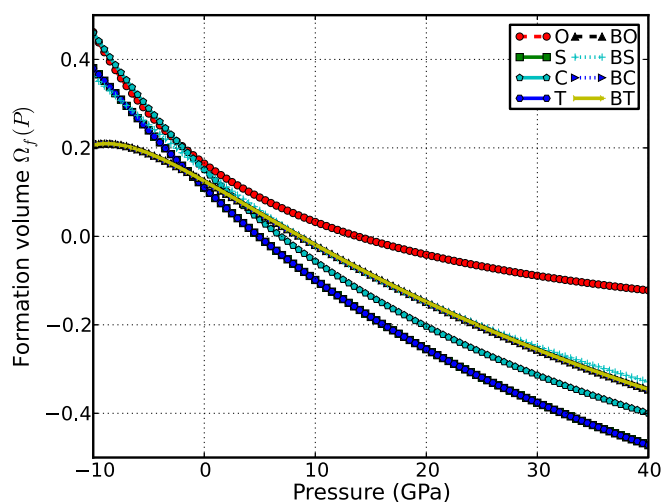


Figure 5 | Formation volume at constant pressure $\Omega^f(P)$ of eight SIAs (O, S, C, T, BO, BS, BC, BT) as function of pressure P .

Table III | Formation volume $\Omega^f(P = 0)$ from *ab initio* DFT calculations and comparison with previous studies. Units of volumes are in $\Omega_0 = 23.52 \text{ \AA}^3$

	Present	Domain [40]	Ackland [41]	Pasianot [42]	Willaime ^a
O	0.164	0.16	-	0.06	0.17
S	0.110	-0.04	0.2	-0.30	0.04
C	0.151	0.13	0.27	-0.9	0.11
T	0.110	-	-	-	-
BO	0.125	0.14	0.3	-0.23	0.12
BS	0.149	-	0.35	-	0.18
BC	0.125	0.1	0.33	-0.14	0.14
BT	0.125	-	-	-	0.12

^awith SIESTA and 97-atom cells in Ref. 10.

Formation enthalpy. Naturally, the presence of pressure introduces the external work of $P\Omega^f$ according to the formation volume Ω^f . Under pressure P , the thermodynamically relevant quantity which determines the stability under pressure is the formation enthalpy^{16–18}. The formation enthalpy of various SIAs ($H^f(P)$) as a function of pressure P are plotted in Fig. 6. The general trend is that the $H^f(P)$ increases with pressure, followed by a drop after reaching a maximum. In the small pressure regime of $P < 10$ GPa, the increase of formation enthalpy $H^f(P)$ is similar to the increase of formation energy $E^f(P)$, but the rate of increment reduces with respect to an increasing pressure. This behavior occurs because the formation energy does not increase sharply enough to compensate the reduction of formation volume with respect to an increasing pressure.

For off-plane SIAs, the rate of increase of formation enthalpy with the pressure is larger than that of the in-plane SIAs, indicating a larger sensitivity to the pressure. In other words, the in-plane SIAs are more stable with respect to pressure. From the view of formation energy, a SIA generated by radiation will become an in-plane SIA during relaxation due to the energy landscape since BO has the lowest formation energy¹¹. Thus there is a movement from off-plane to in-plane. This picture is still valid from the view of formation enthalpy, where the pressure effect has to be considered. The pressure dependent formation enthalpy could also explain the experimental observation of the alignment of c loops in bands parallel with the basal planes in neutron-irradiated Zr⁴³. Furthermore, the 2D diffusion in-plane will transport the SIA along the basal plane.

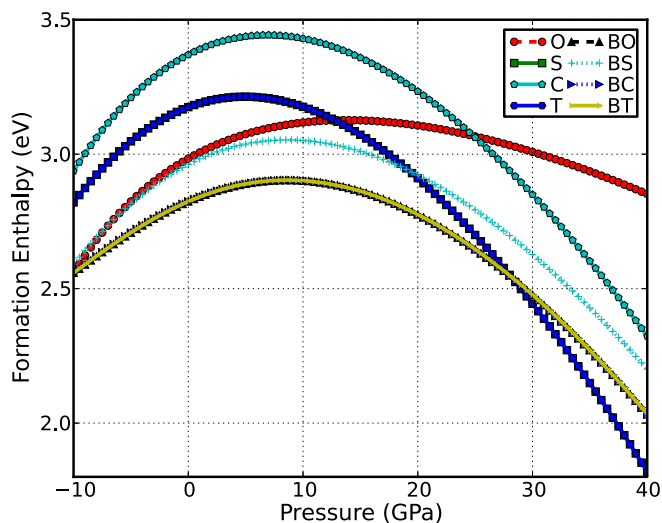


Figure 6 | Formation enthalpy $H^f(P)$ of eight SIAs (O, S, C, T, BO, BS, BC, BT) as a function of pressure P .



This process is repeated until there is a measurable expansion in the a direction and contraction in the c direction, as observed in the single crystal Zirconium⁴⁴. Although dislocation loops, small defect clusters, and dislocation climb processes are responsible for the growth through complex mechanisms, our results suggest a mechanism of radiation growth⁴⁵ caused by 2D diffusion, from the aspect of the stability of the SIAs under pressure. More importantly, our results fit in a recent radiation growth model⁴⁶ in which the radiation growth is governed by the production of SIA clusters and their migration along basal planes. Our results indicate that that under pressures below 12 GPa, the migration and diffusion are still two-dimensional and along basal planes.

In the large pressure regime of $P > 15$ GPa, the formation enthalpy $H^f(P)$ decreases with respect to the pressure. However, the formation energies increase in this regime. Therefore, we can conclude that the external work term of $P\Omega^f$ is dominant under high pressure. For the variation of formation enthalpy to the high pressure, the formation enthalpy $H^f(P)$ decreases, with the slowest corresponding to the O configuration and fastest corresponding to the S configuration.

There are crossovers in these $H^f(P)$ curves: O to BC at $P = 12$ GPa, BS to BC at $P = 20$ GPa, O to C at 25 GPa, and BO to BC at 30 GPa. The crossover of the $H^f(P)$ curves reflects the change of relative stability among the SIAs. Our result shows that the crossovers of $H^f(P)$ curves for different SIAs occur at pressures $P > 12$ GPa and $P = -10$ GPa, which is consistent with the results of $E^f(P)$ and $E^f(\epsilon)$. Since the relative stability of the SIAs affects the diffusion pattern, our results suggest that the diffusion pattern will change under pressures beyond 12 GPa.

It is interesting that the lowest formation enthalpy configuration switches from BO to S at $P = 30$ GPa. This pressure is coincidentally the same as the phase transition pressure of 26–35 GPa from ω phase to β phase. In general, the phase transition follows the path consisted of SIA configurations with low formation enthalpy. Therefore our results could provide a clue to the phase transition path at those pressures, in which the role of SIAs requires further study.

Conclusions

We investigated the equations of state and the effect of pressure on the stability of SIAs in HCP-Zirconium through *ab initio* DFT calculations. We used a generalized EOS method to study the formation energy, formation volume, and formation enthalpy of defects in HCP-Zr. We report that pressure greatly affects the stability and relative stabilities of SIAs. The diffusion and migration patterns are still two-dimensional and along basal planes with pressures below 12 GPa. The formation volumes of SIAs monotonically decrease with an increase in pressure.

In-plane SIAs are more stable with respect to pressures for $P < 10$ GPa. Under high pressures ($P > 15$ GPa), the external work $P\Omega^f$ is dominant compared to the formation energy, leading to the decrease of formation enthalpy. The lowest-conformation-energy configuration changes from BO to O at pressures $P = 21$ GPa with an increase in pressure. There are crossovers in these $H^f(P)$ curves: O to BC at $P = 12$ GPa, BS to BC at $P = 20$ GPa, O to C at 25 GPa, and BO to BC at 30 GPa. The lowest formation enthalpy configuration switches from BO to S at $P = 30$ GPa. The crossovers of the formation enthalpy reflects the changes of the relative stabilities of the SIA configurations, which could provide a clue to phase transitions. Our results indicate that it is important to take the pressure effect into account in predicting the micro-structural evolution of zirconium-based materials under pressure. Our study could be also useful in engineering design of cladding materials and structural materials that are used in the high pressure environment.

1. Sueoka, K., Kamiyama, E. & Kariyazaki, H. A study on density functional theory of the effect of pressure on the formation and migration enthalpies of intrinsic point defects in growing single crystal Si. *J. Appl. Phys.* **111**, 093529 (2012).

2. Kapur, S. S. & Sinno, T. Detailed microscopic analysis of self-interstitial aggregation in silicon. i. direct molecular dynamics simulations of aggregation. *Phys. Rev. B* **82**, 045205 (2010).
3. Kapur, S. S., Nieves, A. M. & Sinno, T. Detailed microscopic analysis of self-interstitial aggregation in silicon. ii. thermodynamic analysis of single clusters. *Phys. Rev. B* **82**, 045206 (2010).
4. Woo, C. H. Modeling irradiation growth of zirconium and its alloys. *Rad. Eff. Def. in Solids* **144**, 145–169 (1998).
5. Wenk, H.-R., Kaercher, P., Kanitpanyacharoen, W., Zepeda-Alarcon, E. & Wang, Y. Orientation relations during the $\alpha - \omega$ phase transition of zirconium: In situ texture observations at high pressure and temperature. *Phys. Rev. Lett.* **111**, 195701 (2013).
6. Wang, B.-T., Zhang, P., Liu, H.-Y., Li, W.-D. & Zhang, P. First-principles calculations of phase transition, elastic modulus, and superconductivity under pressure for zirconium. *J. Appl. Phys.* **109**, 063514 (2011).
7. Johnson, R. A. & Beeler, J. R. *Interatomic Potentials and Crystalline Defects*, 165 (AIME, New York, 1981).
8. Peng, Q., Ji, W., Huang, H. & De, S. Stability of self-interstitials in hcp-Zr. *J. Nucl. Mater.* **429**, 233–236 (2012).
9. Samolyuk, G. D., Golubov, S. I., Osetsky, Y. N. & Stoller, R. E. Self-interstitial configurations in hcp zr: a first principles analysis. *Philos. Mag. Lett.* **93**, 93–100 (2013).
10. V erit e, G. *et al.* Self-interstitial defects in hexagonal close packed metals revisited: Evidence for low-symmetry configurations in Ti, Zr, and Hf. *Phys. Rev. B* **87**, 134108 (2013).
11. Peng, Q., Ji, W., Huang, H. & De, S. Axial ratio dependence of the stability of self-interstitials in hcp structures. *J. Nucl. Mater.* **437**, 293–296 (2013).
12. Xia, H., Ducloux, S. J., Ruoff, A. L. & Vohra, Y. K. New high-pressure phase transition in zirconium metal. *Phys. Rev. Lett.* **64**, 204–207 (1990).
13. Xia, H., Ruoff, A. L. & Vohra, Y. K. Temperature dependence of the ω -bcc phase transition in zirconium metal. *Phys. Rev. B* **44**, 10374–10376 (1991).
14. Dudarev, S. L. Density functional theory models for radiation. *Annu. Rev. Mater. Res.* **43**, 35–61 (2013).
15. Peng, Q., Ji, W. & De, S. First-principles study of the effects of mechanical strains on the radiation hardness of hexagonal boron nitride monolayers. *Nanoscale* **5**, 695–703 (2013).
16. Mukherjee, S., Cohen, R. E. & Gulseren, O. Vacancy formation enthalpy at high pressures in tantalum. *J. Phys.:Condens. Matter* **15**, 855–861 (2003).
17. Ho, G., Ong, M. T., Caspersen, K. J. & Carter, E. A. Energetics and kinetics of vacancy diffusion and aggregation in shocked aluminium via orbital-free density functional theory. *Phys. Chem. Chem. Phys.* **9**, 4951–4966 (2007).
18. Chen, Z., Kioussis, N., Ghoniem, N. & Seif, D. Strain-field effects on the formation and migration energies of self interstitials in alpha-fe from first principles. *Phys. Rev. B* **81**, 094102 (2010).
19. Kresse, G. & Hafner, J. *Ab initio* molecular dynamics for liquid metals. *Phys. Rev. B* **47**, 558–561 (1993).
20. Kresse, G. & Furthm uller, J. Efficient iterative schemes for *ab initio* total-energy calculations using a plane-wave basis set. *Phys. Rev. B* **54**, 11169–11186 (1996).
21. Murnaghan, F. D. The compressibility of media under extreme pressures. *Proc. Natl. Acad. Sci. USA* **30**, 244–247 (1944).
22. Vinet, P., Smith, J. R., Ferrante, J. & Rose, J. H. A universal equation of state for solids. *J. Phys. C* **19**, L467 (1986).
23. Vinet, P., Smith, J. R., Ferrante, J. & Rose, J. H. Temperature effects on the universal equation of state of solids. *Phys. Rev. B* **35**, 1945–1953 (1987).
24. Jeanloz, R. Universal equation of state. *Phys. Rev. B* **38**, 805–807 (1988).
25. Cohen, R. E., Gulseren, O. & Hemley, R. J. Accuracy of equation-of-state formulations. *Am. Mineral.* **85**, 338–344 (2000).
26. Tyuterev, V. G. & Vast, N. Murnaghans equation of state for the electronic ground state energy. *Comput. Mat. Sci.* **38**, 350–353 (2006).
27. Malerba, L. *et al.* *Ab initio* calculations and interatomic potentials for iron and iron alloys: Achievements within the perfect project. *J. Nucl. Mater.* **406**, 7–18 (2010).
28. Kohn, W. & Sham, L. J. Self-consistent equations including exchange and correlation effects. *Phys. Rev.* **140**, A1133–A1138 (1965).
29. Perdew, J. P., Burke, K. & Ernzerhof, M. Erratum: Generalized gradient approximation made simple. *Phys. Rev. Lett.* **78**, 1396 (1997).
30. Kresse, G. & Joubert, D. From ultrasoft pseudopotentials to the projector augmented-wave method. *Phys. Rev. B* **59**, 1758–1775 (1999).
31. Methfessel, M. & Paxton, A. T. High-precision sampling for brillouin-zone integration in metals. *Phys. Rev. B* **40**, 3616–3621 (1989).
32. Le Page, Y. & Saxe, P. Symmetry-general least-squares extraction of elastic data for strained materials from *ab initio* calculations of stress. *Phys. Rev. B* **65**, 104104 (2002).
33. Steinle-Neumann, G., Stixrude, L. & Cohen, R. E. First-principles elastic constants for the hcp transition metals Fe, Co, and Re at high pressure. *Phys. Rev. B* **60**, 791–799 (1999).
34. Vaidya, S. N. & Kennedy, G. C. Compressibility of 22 elemental solids to 45 KB. *J. Phys. Chem. Solids* **33**, 1377–1389 (1972).
35. Zhao, Y. *et al.* Thermal equations of state of the α , β , and ω phases of zirconium. *Phys. Rev. B* **71**, 184119 (2005).
36. Schnell, I. & Albers, R. C. Zirconium under pressure: phase transitions and thermodynamics. *J. Phys.:condens. matter* **18**, 1483 (2006).



37. Zhang, S. *et al.* First-principles study on the structural stabilities, electronic and elastic properties for zirconium under pressure. *Comput. Mater. Sci.* **50**, 179–183 (2010).
38. Gillan, M. J. Calculation of the vacancy formation energy in aluminum. *J. Phys.-Cond. Mat.* **1**, 689 (1989).
39. Willaime, F. Ab initio study of self-interstitials in hcp-Zr. *J. Nucl. Mater.* **323**, 205–212 (2003).
40. Domain, C. & Legris, A. Ab initio atomic-scale determination of point-defect structure in hcp zirconium. *Philos. Mag.* **85**, 569–575 (2005).
41. Ackland, G. J., W. S. J. & J. B. D. Defect, surface and displacement-threshold properties of alpha-zirconium simulated with a many-body potential. *Philos. Mag. A* **71**, 553–565 (1995).
42. Pasianot, R. & Monti, A. A many body potential for α -Zr. Application to defect properties. *J. Nucl. Mater.* **264**, 198–205 (1999).
43. Griffiths, M. A review of microstructure evolution in zirconium alloys during irradiation. *J. Nucl. Mater.* **159**, 190–218 (1988).
44. Northwood, D. & Herring, R. Irradiation growth of zirconium alloy nuclear reactor structural components. *J. Mater. Energy Systems* **4**, 195–216 (1983).
45. Woo, C. H. & Liu, X. Atomistic calculation of point-defect diffusion anisotropy and irradiation growth in alpha-zirconium. *Philos. Mag.* **87**, 2355–2369 (2007).
46. Golubov, S. I., Barashev, A. & Stoller, R. E. *On the origin of radiation growth of hcp crystals* (2012). DOI:10.2172/1037031.
47. Fisher, E. S. & Renken, C. J. Single-crystal elastic moduli and the hcp \rightarrow bcc transformation in Ti, Zr, and Hf. *Phys. Rev.* **135**, A482–A494 (1964).
48. Hao, Y.-J., Zhang, L., Chen, X.-R., Li, Y.-H. & He, H.-L. Phase transition and elastic constants of zirconium from first-principles calculations. *J. Phys.-condens. matter* **20**, 235230 (2008).
49. Mendelev, M. I. & Ackland, G. J. Development of an interatomic potential for the simulation of phase transformations in zirconium. *Philos. Mag. Lett.* **87**, 349–359 (2007).

Acknowledgments

Q.P. and S.D. would like to acknowledge the generous financial support from the Defense Threat Reduction Agency (DTRA) Grant # BRBAA08-C-2-0130 and # HDTRA1-13-1-0025. W.J. thanks the U.S. Nuclear Regulatory Commission Faculty Development Program under contract # NRC-38-08-950 and # NRC-38-09-954, and U.S. Department of Energy (DOE) Nuclear Energy University Program (NEUP) Grant # DE-NE0000325 for support of this work. F. Gao is grateful for the support by the US Department of Energy, Office of Nuclear Energy (Nuclear Energy University Program), under Contract DE-AC06-76RLO 1830.

Author contributions

Q.P., H.H. and S.D. designated the research topic. Q.P. and W.J. carried out the calculations. Q.P., X.C., J.L. and F.G. did the analysis. Q.P. wrote the main manuscript text and designed the figures. All authors discussed the results and commented on the manuscript.

Additional information

Competing financial interests: The authors declare no competing financial interests.

How to cite this article: Peng, Q. *et al.* Pressure effect on stabilities of self-Interstitials in HCP-Zirconium. *Sci. Rep.* **4**, 5735; DOI:10.1038/srep05735 (2014).



This work is licensed under a Creative Commons Attribution-NonCommercial-NoDerivs 4.0 International License. The images or other third party material in this article are included in the article's Creative Commons license, unless indicated otherwise in the credit line; if the material is not included under the Creative Commons license, users will need to obtain permission from the license holder in order to reproduce the material. To view a copy of this license, visit <http://creativecommons.org/licenses/by-nc-nd/4.0/>